Brain (2001), **124,** 893–906

Anti-GQ1b ganglioside antibodies mediate complement-dependent destruction of the motor nerve terminal

Graham M. O'Hanlon,[1] Jaap J. Plomp,[2,3] Mahua Chakrabarti,[1] Ian Morrison,[1] Eric R. Wagner,[1] Carl S. Goodyear,[1,4] Xinghua Yin,[5] Bruce D. T. Trapp,[5] Joe Conner,[4] Peter C. Molenaar,[2] Suzanne Stewart,[6] Edward G. Rowan[6] and Hugh J. Willison[1]

[1]*University Department of Neurology, Institute of Neurological Sciences, Southern General Hospital,* [4]*Department of Biological Sciences, Glasgow Caledonian University,* [6]*Department of Physiology and Pharmacology, University of Strathclyde, Glasgow, UK, Departments of* [2]*Physiology and* [6]*Neurology, Leiden University Medical Centre, The Netherlands and* [5]*Neurosciences/NC30, Lerner Research Institute, Cleveland Clinic Foundation, Cleveland, Ohio, USA*

Correspondence to: Dr Hugh J. Willison, University Department of Neurology, Southern General Hospital, Glasgow G51 4TF, UK
E-mail: h.j.willison@udcf.gla.ac.uk

Summary

Miller–Fisher syndrome is an autoimmune neuropathy characterized by ataxia, areflexia and ophthalmoplegia, and in the majority of cases the presence of high titres of anti-GQ1b ganglioside antibodies. In an *ex vivo* model, human and mouse anti-GQ1b antibodies have been shown previously to induce a complement-dependent α-latrotoxin-like effect on the murine motor endplate, i.e. they bring about massive quantal release of acetylcholine and eventually block neuromuscular transmission. Using immunofluorescence microscopy with image analysis, we show here that the late stages of this electrophysiological effect temporally coincide with the loss of heavy neurofilament (200 kDa) and type III β-tubulin immunostaining and structural breakdown of the nerve terminal, as demonstrated by electron microscopy. Ultrastructurally, axon terminals were disorganized, depleted of vesicles, and subdivided by the infiltrating processes of capping Schwann cells. These findings provide clear pathological evidence to support a role for anti-ganglioside antibodies in mediating nerve terminal injury and further advance the view that this site may be of importance as a target in some human neuropathies.

Keywords: autoantibody; complement; ganglioside; Miller–Fisher syndrome; neuromuscular junction

Abbreviations: BTx = α-bungarotoxin; EM = electron microscopy; MFS = Miller–Fisher syndrome; JF = junctional folds; LTx = α-latrotoxin; mAb = monoclonal antibody; NF = neurofilament; NMJ = neuromuscular junction; PBS = phosphate-buffered saline

Introduction

The Miller–Fisher syndrome (MFS) variant of Guillain–Barré syndrome is characterized by ataxia, areflexia and ophthalmoplegia. Over 90% of MFS cases have acute phase anti-GQ1b ganglioside antibodies, which are particularly associated with ophthalmoplegic disease (Chiba *et al.*, 1992, 1993; Willison *et al.*, 1993; Suzuki *et al.*, 1998). The majority of MFS-associated anti-GQ1b antibodies cross-react with GT1a and 50% react with other disialylated gangliosides including GD3 and GD1b (Willison *et al.*, 1994). The enrichment of GQ1b in human extraocular nerves compared with limb nerves may account, at least in part, for the anatomical specificity of paralysis (Chiba *et al.*, 1997).

MFS is a post-infectious illness which may be preceded by *Campylobacter jejuni* enteritis, and antigen mapping and structural studies have demonstrated that GT1a and GD3-like disialylated oligosaccharides are present in lipopolysaccharides from MFS-associated *C. jejuni* serostrains (Jacobs *et al.*, 1995, 1997; Salloway *et al.*, 1996; Yuki, 1998). It is thus likely that molecular mimicry between microbial and neural oligosaccharides accounts for the serospecificity

seen in MFS (Yuki *et al.*, 1994; Penner and Aspinall, 1997). In support of this, we have recently demonstrated serological cross-reactivity between gangliosides and lipopolysaccharides in mice immunized with *C. jejuni* lipopolysaccharides bearing disialylated ganglioside-like motifs. From seropositive animals we have cloned a series of anti-GQ1b/GD3/GT1a monoclonal antibodies (mAbs) (Goodyear *et al.*, 1999).

Our previous experimental studies and those of Buchwald *et al*. (1995, 1998), on the pathogenic effects of anti-GQ1b antibodies in MFS have focused on the neuromuscular junction (NMJ) as one of the many potential sites of immunopathology. The NMJ is rich in gangliosides, lies outside the blood–nerve barrier, and is an important site of other antibody-mediated autoimmune diseases. In addition, it is the site of action of botulinum toxins, which produce a disorder of synaptic transmission (botulism) clinically resembling MFS, in which gangliosides act, in part, as presynaptic ectoacceptors for the bacterial toxin(s) (Fishman *et al.*, 1993). Furthermore, there is some indirect clinical electrophysiological evidence of NMJ involvement in MFS (Uncini and Lugaresi, 1999).

Using the *ex vivo* mouse phrenic nerve hemi-diaphragm preparation as a model system to monitor nerve terminal injury, we have shown previously that MFS sera containing polyclonal anti-GQ1b antibodies, MFS IgG, a human anti-GQ1b IgM mAb [termed Ha1 and cloned from a chronic MFS-like case (Willison *et al.*, 1996)] and mouse anti-GQ1b mAbs bind at the mouse NMJ. At this site, they each induce massive and rapid asynchronous quantal release of acetylcholine and eventually block neuromuscular transmission (Goodyear *et al.*, 1999; Plomp *et al.*, 1999; Bullens *et al.*, 2000). Although this *ex vivo* mouse model is clearly incomplete with respect to reproducing the chain of events occurring in the human disease, it remains the best currently available system in which to study the pathophysiological effects of anti-GQ1b antibodies. The electrophysiological effect observed *ex vivo* is complement dependent, closely resembles that of the paralytic spider neurotoxin, α-latrotoxin (Plomp *et al.*, 1999) and also has some features of the effect of toxins with phospholipase A2 activity, such as the krait snake toxin β-bungarotoxin (Masukawa and Livengood, 1982). Immunohistological analysis of paralysed tissues reveals deposits of immunoglobulin, the complement product C3c (Goodyear *et al.*, 1999; Plomp *et al.*, 1999) and membrane attack complex (our unpublished observations) at the NMJ. In humans developing MFS, these rapid onset toxin-like effects are not known to occur. This may be due to a much slower rate of accumulation (and/or faster clearance) of antibody and complement products at extraocular nerve terminals, compared with this acute exposure *ex vivo* model.

Both activated complement and α-latrotoxin (LTx) are thought to form pores in target membranes, which allow the entry of calcium (Zalman and Muller-Eberhard, 1990; Pashkov *et al.*, 1993) and may lead to pleiotropic intraterminal effects, including the activation of calcium-dependent proteolytic enzymes such as the neutral protease calpain. This enzyme can cleave a variety of cytoskeletal proteins including fodrin (Siman *et al.*, 1984), spectrin (Billger *et al.*, 1988; Seubert *et al.*, 1988; Roberts-Lewis and Siman, 1993), tubulin (De Freitas *et al.*, 1996) and neurofilament (Pant, 1988). The aim of this study was to determine whether any morphological abnormalities could be detected at the motor nerve terminal either as a consequence of, or occurring in parallel with, the previously observed electrophysiological effects of anti-GQ1b antibodies. Such information could provide insights into the mechanism(s) of anti-GQ1b antibody dependent complement-mediated injury to the distal motor axon. Furthermore, it may provide a model system for assessing therapeutic factors that might attenuate such effects. In NMJs, the terminal arborization, a branched extension of the axon extending through the endplate region, contains neurofilaments and the neurone-associated type III β-tubulin. If complement-mediated injury leads to nerve terminal disruption at the motor nerve terminal, then loss of structural proteins should be observed on immunohistological analysis. We therefore investigated both the gross morphology of the motor nerve terminal in anti-GQ1b antibody- and complement-treated tissue using immunofluorescence microscopy of cytoskeletal proteins and synaptic ultrastructure using electron microscopy (EM).

Material and methods

Antibodies

The IgM anti-ganglioside mAb CGM3 was derived from mice inoculated with *C. jejuni* lipopolysaccharide, and reacts with the gangliosides GQ1b, GD3 and GT1a (Goodyear *et al.*, 1999), but not GM1 and GD1a. mAb 22/18, a mouse IgM reactive with a non-ganglioside carbohydrate cell-marker present in the newt, was used as an mAb control, and was found not to accumulate at the NMJ, in contrast to the anti-GQ1b mAbs (Goodyear *et al.*, 1999). Hybridoma cells producing 22/18, developed by Brockes (Kintner and Brockes, 1985), were obtained from the Developmental Studies hybridoma bank maintained by the University of Iowa Department of Biological Sciences (Iowa City, IA) under contract NO1-HD-7-3263 from the National Institute of Child Health and Human Development. mAb concentrations were measured using a radial immunoglobulin diffusion kit (Binding Site, Birmingham, UK), and they were diluted and dialysed in Ringer prior to use. Serum MFS1 was collected from a patient with MFS as described previously (Plomp *et al.*, 1999).

Tissue preparation and qualitative assessment of neuromuscular function

Hemi-diaphragms were prepared from male Swiss mice aged 3–4 weeks (12–15 g), and paired experimental and control

incubations were conducted on hemi-diaphragms derived from the same animal (Plomp *et al.*, 1999). Each condition was repeated three times, and in each case the allocation of left and right hemi-diaphragm to experimental and control groups was reversed. Test solutions comprised heat-inactivated and defibrinated MFS1 serum (Plomp *et al.*, 1999) diluted 1 : 2 in Ringer, heat-inactivated normal human serum (defibrinated, diluted 1 : 2), CGM3 (50 μg/ml) and 22/18 (50 μg/ml). Solutions were dialysed overnight in Ringer prior to use.

Hemi-diaphragms were incubated with test solutions for 3 h at 32°C, followed by 30 min at 8°C, performed in view of the facilitated antigen binding of some anti-ganglioside antibodies at a lower temperature. The preparations were rinsed briefly in Ringer at room temperature, then incubated with normal human serum (1 : 2) for 1 h, also at room temperature, from a stock that was freshly frozen and stored in aliquots at –80°C (Plomp *et al.*, 1999).

During this last incubation period, each preparation was inspected visually under the stereomicroscope (×40), and was scored on spontaneous asynchronous contractile activity and on the tetanic contraction upon supramaximal electrical stimulation of the phrenic nerve (3 V, 0.1 ms duration, 40 Hz for ~1 s). For spontaneous activity, the tissue scored 0 for no activity, 1 for the twitching of ⩽10 fibres, 2 for a small amount of twitching across the tissue, 3 for a moderate amount and 4 for an extensive amount. Nerve stimulation-evoked contraction was scored 2 for a contraction of the whole muscle preparation, 1 for a partial contraction and 0 for no contraction. Where incubated tissue approached an evoked contraction score of 0, the viability of the muscle was confirmed by observing contraction induced by direct muscle stimulation with needle electrodes (10 V, 1 ms duration, 40 Hz for ~1 s). All incubations were terminated 1 h after the addition of fresh human serum, irrespective of the state of neuromuscular transmission. In order to provide tissue suitable for comparative morphological analysis, the two hemi-diaphragms from one mouse were treated with LTx (10 nM, Alomone Laboratories, Jerusalem, Israel) in Ringer solution and maintained at room temperature for 90 min, during which time similar qualitative assessments were made.

Tissue samples for immunofluorescence studies

Hemi-diaphragms exposed to the organ bath conditions described above were first washed in Ringer solution for 15 min. The dorsal half of each preparation was then snap-frozen on dry ice for immunofluorescence studies. For neurofilament analysis, unfixed tissue samples were mounted in Lipshaw's M-1 mounting medium (Pittsburgh, Pa., USA) and cryostat sections (7 μm) were cut onto 3-aminopropyltriethoxysilane-coated slides and allowed to air-dry before use or storage at –20°C. Samples consisting of one specimen from each experimental category were coded and the assessments were conducted blind. A second series of hemi-diaphragm tissue samples from one of each experimental condition was fixed in 4% paraformaldehyde for 1 h at 4°C, rinsed in phosphate-buffered saline (PBS) for 30 min and then processed as above.

Complement immunostaining

In order to identify complement deposition at the NMJ, unfixed tissue sections were incubated with FITC (fluorescein isothiocyanate)-labelled anti-complement C3c (diluted 1 : 300; Dako, Ely, UK) in PBS containing 10% goat serum. To localize NMJs, rhodamine labelled α-bungarotoxin (BTx; diluted 1 : 200; Molecular Probes, Leiden, The Netherlands), which binds to post-synaptic acetylcholine receptors, was also included. The sections were incubated for 1 h at 4°C, rinsed, and mounted in Citifluor antifade (Citifluor Products, Canterbury, UK).

Cytoskeletal immunostaining

Three anti-200 kDa neurofilament (NF) antibodies were used: the mouse mAb 1217 (clone SMI 32; Affiniti Research Products Ltd, Exeter, UK) reactive with non-phosphorylated NF (diluted 1 : 750), the mouse mAb 2F11 (Dako) reactive with phosphorylated NF (diluted 1 : 50), and the rabbit polyclonal serum 1211 (Affiniti) also reactive with highly phosphorylated NF (diluted 1 : 750). Sections of unfixed tissue were incubated at room temperature overnight with primary antibodies in a staining solution of PBS containing 10% goat serum and 0.1% Triton X-100. Sections were drained, rinsed four times in cold PBS and incubated with FITC-labelled goat anti-mouse or anti-rabbit IgG secondary antibody (Southern Biotechnology Associates, Birmingham, Ala., USA) at 1 : 300 dilution in PBS containing BTx as above, for 1 h at 4°C. The slides were again rinsed four times in cold PBS and mounted. In some instances muscle sections were incubated overnight at room temperature with alkaline phosphatase (400–1000 U/ml; Sigma, Poole, UK) in 0.1 M Tris-buffered saline pH 8 containing anti-NF antibodies (1217 and 2F11) and 0.1% Triton X-100 as above. The slides were rinsed, exposed to secondary antibody and mounted as above.

The staining of β-tubulin was assessed on fixed tissue sections from the same hemi-diaphragm preparations used for the neurofilament analysis. Staining was conducted using mouse anti type III β-tubulin (Promega, Madison, Wis., USA; diluted 1 : 500). Incubation conditions, secondary antibodies and BTx were applied as for NF.

Image acquisition

Digital images were captured by a Sony colour CCD camera mounted onto a Zeiss Axioplan fluorescent microscope and linked to a PC-driven image archiving system (Sirius VI; Optivision, Ossett, UK). Some illustrative images were obtained on a Bio-Rad MRC600 or Zeiss Pascal confocal microscope.

Image analysis measurements were made using Aequitas

IA image analysis software (Dynamic Data Links Ltd, Cambridge, UK). Bitmap processing and annotation were conducted on PhotoMagic (Micrographx Inc., Richardson, Tex., USA) and Powerpoint (Microsoft). Images were printed directly using a photographic-quality colour printer (Epson Photostylus).

Image analysis of the NMJ

NMJs were identified on the basis of BTx staining, and under standardized camera conditions, images of the BTx and associated cytoskeletal stain were recorded. The processing of an illustrative NMJ image is shown in Fig. 1A. Using the Sirius image processing and archiving system, the red-plane (BTx; Fig. 1C) was converted into a negative black-and-white image and then transformed into a 'filter' (grey scale = background, black = BTx; Fig. 1D). This required operator selection of the black cut-off level according to the perceived limit of the BTx staining. To isolate NMJ-associated cytoskeletal staining, the filter was subtracted from the green plane, leaving only the signal located directly above that of the BTx (Fig. 1E). This was defined as the terminal signal. Using Aequitas image analysis software, the black region of the filter (Fig. 1D) was used to determine the BTx area. The area of the terminal signal was also measured, using a predetermined threshold to cut out low-level background signals (Fig. 1F). In the resultant data, the terminal signal area was expressed as a percentage of the BTx region. Since this figure was subject to inter-experimental variability, and ultimately dependent on a variety of technical settings which changed with the different antibodies, limited inference could be made from the absolute value. As a result, after sample decoding, this value was converted to a percentage of the mean value for the combined control tissues. For NF studies, a total of 691 NMJs were sampled from four separate staining procedures. For β-tubulin studies, a total of 893 NMJs were sampled from five separate staining procedures.

Similar procedures were employed to determine the amount of complement C3c deposited at the NMJ, but since the values for control samples were close or equal to zero, the levels at mAb-treated endplates were expressed in absolute terms rather than a percentage of the controls. For C3c studies, a total of 185 NMJs were sampled from a single staining procedure.

Electron microscopy

Half of each hemi-diaphragm was fixed *in situ* (i.e. whilst pinned out) with 2% paraformaldehyde/2.5% glutaraldehyde for 1 h at 8°C. The tissue was rinsed and stored in PBS prior to embedding. The EM samples were coded at the embedding stage, and subsequent morphological analyses were conducted blind. Tissue samples were prepared for EM analysis using standard procedures. Briefly, fixed tissue was treated with 1% osmium tetroxide for 45 min, rinsed, and taken through a series of graded alcohols (25, 50, 75 and 100%; 2 × 10 min each), before treatment with 100% propylene oxide (2 × 10 min). After infiltration with propylene oxide/Araldite 1 : 1 for 4 h and 1 : 3 for 4 h, the tissue was placed in mould with fresh Araldite and cured overnight at 60°C.

Semi-thin sections (0.5–1 μm), stained with toluidine blue, were used to identify the NMJ-containing region of the muscle, from which ultra-thin sections (80–100 nm) were then cut. The sections were mounted onto copper grids and stained with 5% uranyl acetate and Reynolds lead citrate prior to viewing.

Ultrastructural quantification

NMJs were identified by the presence of post-synaptic junctional folds (JF), photographed at ×10 000 and ×30 000 magnification and the images used for morphological assessment. Individual NMJs were scored (present = 1 or absent = 0) for: (i) damaged mitochondria; (ii) the presence of JF with no apposed presynaptic structure; (iii) JF apposed by Schwann cell processes; (iv) the presence of nerve terminal profiles completely separated from the muscle by Schwann cell processes ('full wrap'); and (v) the complete absence of a nerve terminal, or its complete separation from muscle by Schwann cell processes ('denervated'). A qualitative score (normal = 1; abnormal = 0) was also assigned to each NMJ based on the observer's overall impression.

Individual NMJs were composed of one or more separate nerve terminal profiles. For individual profiles, a further series of measurements and counts were made. Nerve profile perimeter length and circularity (computer-calculated image analysis functions, the latter measuring approximation to a circle; scored 0–1) were both parameters chosen to provide an index of globular swelling of the terminal. Muscle contact ratio (the length of the nerve–muscle interface as a proportion of the perimeter; scored 0–1) provides quantification of the degree of retraction of the nerve terminal from the muscle surface. The percentage of profiles with damaged mitochondria, and the percentage of damaged mitochondria within a nerve profile both give an indication of the overall integrity of the terminal. Where no mitochondria were observed, no figure was recorded, so the *n* value for this test is less than the number of profiles. The presence of Schwann cell processes within the synaptic cleft, which separate JF from the nerve terminal (scored 1 or 0), and the incidence of a 'full wrap' of Schwann cell processes around the nerve profile (scored 1 or 0) give a measure of the degree to which Schwann cells are involved in the pathological process. Finally, a count of the number of vesicles present in a 200 × 200 nm box placed over the pre-synaptic nerve terminal opposed to the opening of a JF (a position considered to coincide with the active zone) gives an indication of the level of vesicle depletion. The numerical value assigned for each profile was the mean of one to eight counts, and where no JF was observed or the intervening cleft was blocked by Schwann cell processes, no figure was recorded so the *n* value for this test will be less than the number of profiles.

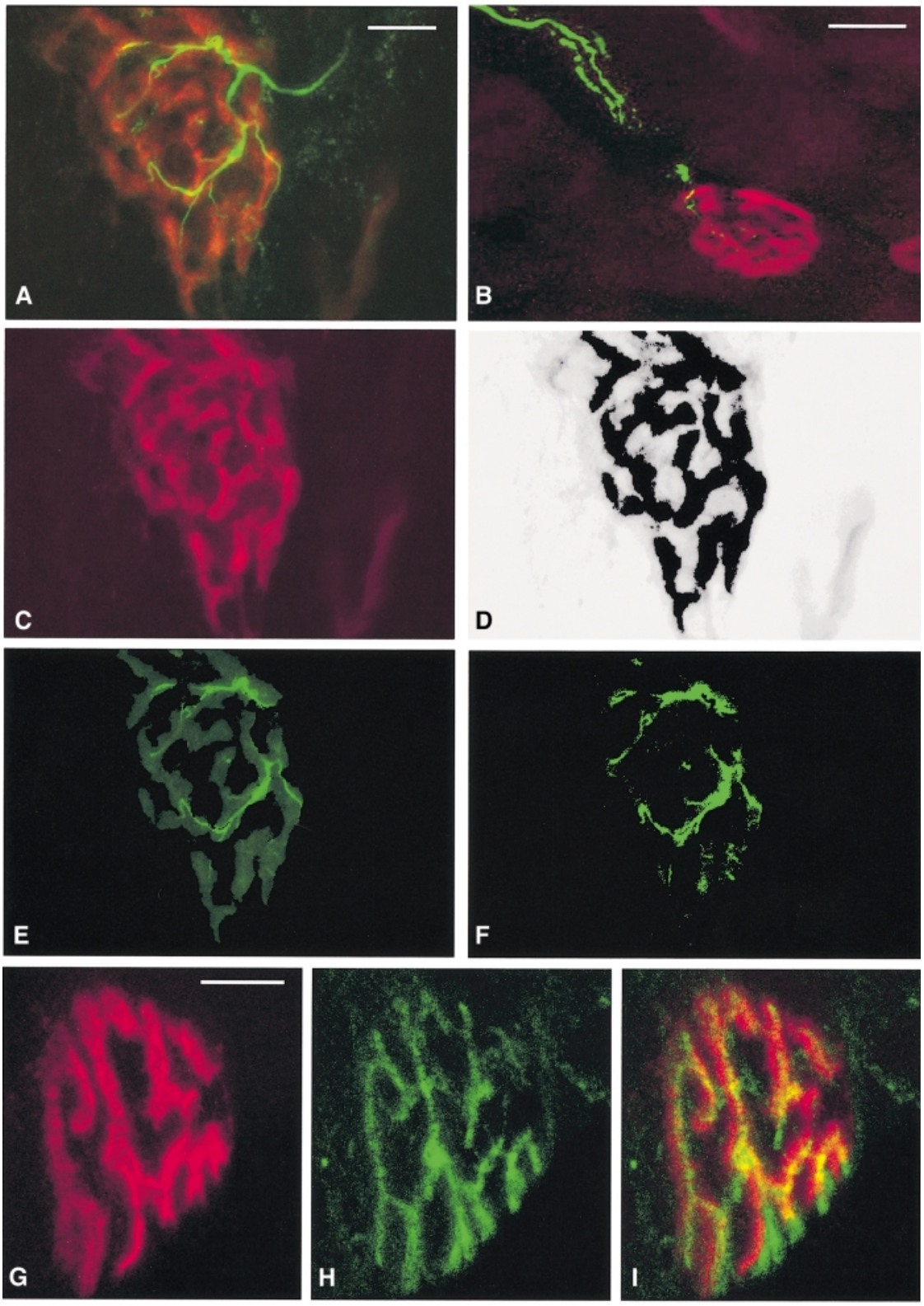

Fig. 1 (**A**) A normal mouse NMJ with the post-junctional acetylcholine receptors stained with BTx (red) and the pre-synaptic, non-phosphorylated NF (green). The NF filaments elaborate a ramified network overlaying the BTx-labelled region. Following treatment with CGM3, there is complement-dependent loss of NF signal (green) over the NMJ (**B**). The proximal axon also appears fragmented. Scale bars = 15 μm in **A**, 25 μm in **B**. Panels **C**–**F** show the image-analysis procedure conducted on the image shown in panel **A**. A filter was created using the BTx image (**C**), such that the black space represents the BTx-positive region (**D**). This was subtracted from the NF signal to leave an image of staining at the NMJ only (**E**). From this image, the area covered by signal over a baseline threshold was measured (**F**), and expressed as a percentage of the BTx area (measured from **D**). Panels **G**–**I** show immunostaining of an NMJ from untreated mouse diaphragm with α-bungarotoxin (**G**) and anti-β-tubulin (**H**). The two labels are overlaid in **I**. Scale bar in **G** = 10 μm.

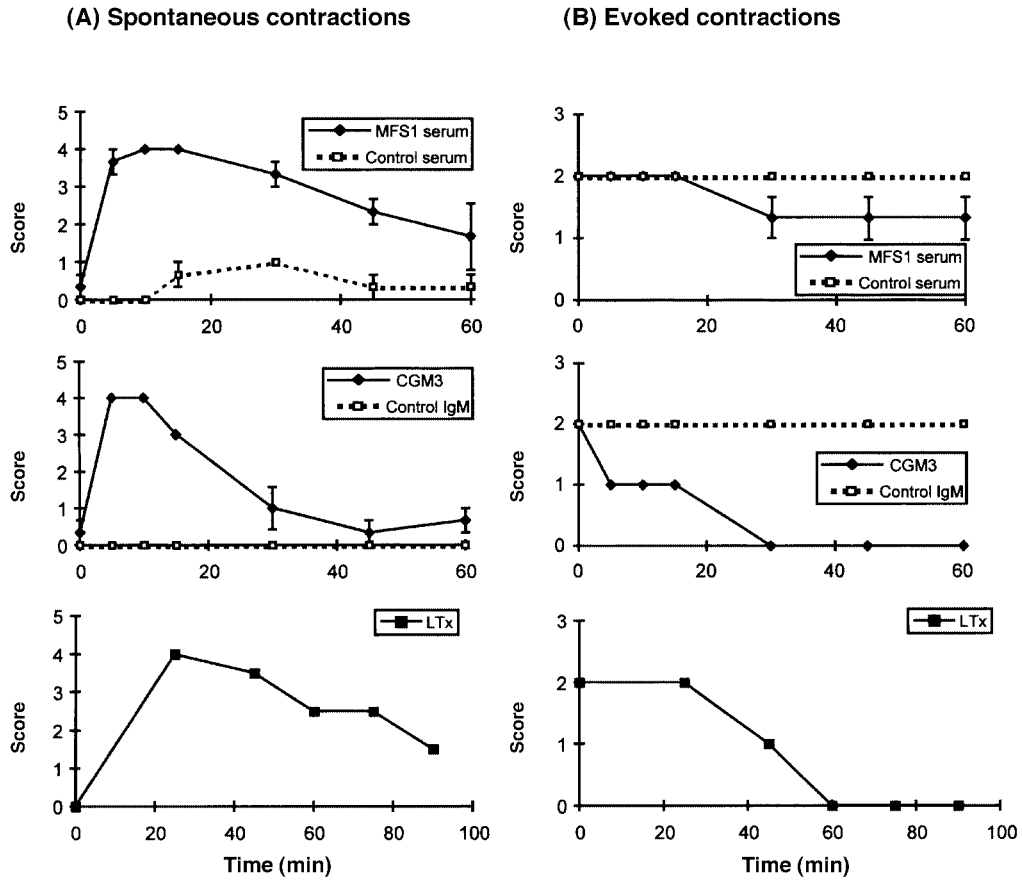

Fig. 2 (**A**) Qualitative scoring of spontaneous asynchronous contractile activity in hemi-diaphragm preparations: 0 = none, 1 = <10 fibres, 2 = little, 3 = moderate, 4 = extensive. Figures are the mean of observations made from three different muscles (two for LTx) ± standard error of the mean. In anti-ganglioside antibody-treated tissue, there is a rapid rise in spontaneous contractile activity, and this is still evident, though diminished after 60 min. Since a pre-incubation period is not possible with LTx, there is a slower rise time in spontaneous activity as the ligand diffuses into the tissue. (**B**) Scoring of the proportion of tetanic contraction of the hemi-diaphragm preparation upon supramaximal electrical stimulation of the phrenic nerve: 0 = none, 1 = part, 2 = whole. Whereas CGM3 treatment produced complete paralysis of the tissue by 30 min, only a partial paralysis was achieved after 60 min in MFS1-treated tissue. LTx produced compete paralysis by 60 min. Control tissue remained fully responsive to such stimulation.

Results

Electrophysiological lesion

The progress of the electrophysiological lesion was assessed by visual scoring of spontaneous asynchronous contractile activity, and on the tetanic contraction upon supramaximal electrical stimulation of the phrenic nerve of each hemi-diaphragm preparation (Fig. 2). In all hemi-diaphragms pre-exposed to anti-GQ1b antibody containing samples, spontaneous contractions began shortly after the addition of the complement source (human serum). As previously reported, contractions were declining by 30 min, at which time the CGM3-treated tissue had become completely refractory to nerve stimulation throughout the hemi-diaphragm. By 1 h after the addition of the complement source, the MFS1-treated hemi-diaphragms had not become uniformly and completely paralysed, but towards the end of the incubation large bundles of fibres were observed to be without contractions during evoked stimulation.

As seen with CGM3, LTx-treated tissue displayed abundant spontaneous contractions, which were still apparent at the time when the preparation was refractory to phrenic nerve stimulation.

Complement activation

Tissue samples were analysed for the deposition of complement cleavage product C3c at the NMJ (Fig. 3). Only 2% of the 88 NMJs sampled from control tissue demonstrated C3c staining, compared with 31 and 98% for MFS1- (n = 42) and CGM3-treated tissue (n = 55), respectively. In comparison with CGM3-treated tissue, the deposits on MFS1-treated NMJ covered a smaller area. Thus, the tissues showing lower levels of complement activation correspond to the treatment that produced the more modest electrophysiological effects (see Fig. 2).

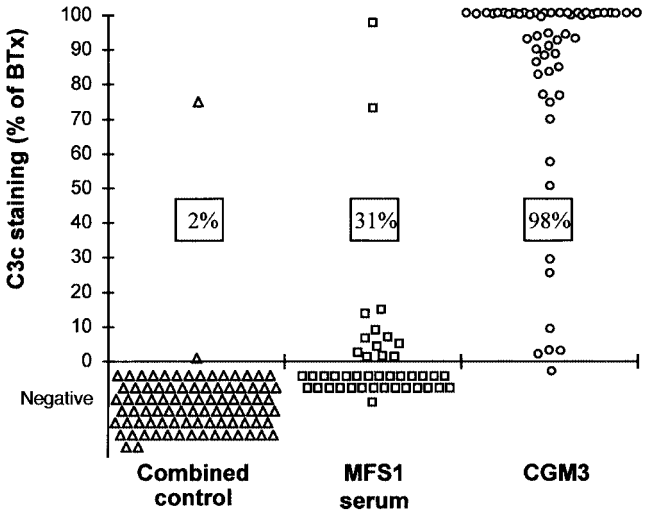

Fig. 3 Analysis of complement C3c deposition at the NMJ. Graphs show the results of NMJs positive for C3c. The boxed figures are the percentage of total NMJs displaying a positive complement signal, i.e. an NMJ with a C3c signal that exceeds pre-set imaging thresholds (C3c/BTx > 0). The deposits on CGM3-treated NMJs were significantly stronger, i.e. covering more of the endplate region than those of MFS1-treated tissue. Sample sizes: combined control (normal human serum + 22/18), $n = 88$; MFS1, $n = 42$; CGM3, $n = 55$.

Neurofilament changes at the NMJ

Immunostaining of normal mouse hemi-diaphragm reveals a ramified 'footprint' of non-phosphorylated NF labelling over the endplate region as delineated by BTx staining (Fig. 1A). As observed by others (Yee *et al.*, 1988), the NF bundles typically occupied a minority of the area delineated by BTx, with the remainder of the space being occupied by other components of the pre-synaptic apparatus. Because of the diversity of NMJ orientations presented in tissue sections, a positive signal was not observed at every endplate. However, compared with control samples, the NF signal at the NMJ in anti-GQ1b mAb- and complement-treated samples appeared diminished or lost, even though NF staining in associated intra-muscular nerve fibres and bundles was still evident. To quantify this apparent NF loss at the end plate, an image analysis method was developed using principles similar to those described previously (Prakash *et al.*, 1996) (Fig. 1).

We assessed the phosphorylated NF signal in mouse diaphragm nerve terminals incubated with anti-GQ1b or control antibodies and complement (Fig. 4). In anti-ganglioside antibody-treated diaphragms, there was a significant reduction in the proportion of the NMJ occupied by an NF signal (Student's two-tailed *t*-test, $P < 0.01$). Similar losses of NF staining were also demonstrated (data not shown) with other antibodies reactive with phosphorylated NF (2F11) and with an antibody reactive with non-phosphorylated NF (1217). In tissue treated with CGM3 alone, i.e. in the absence of a source of complement, there was no loss of NF staining (data not shown).

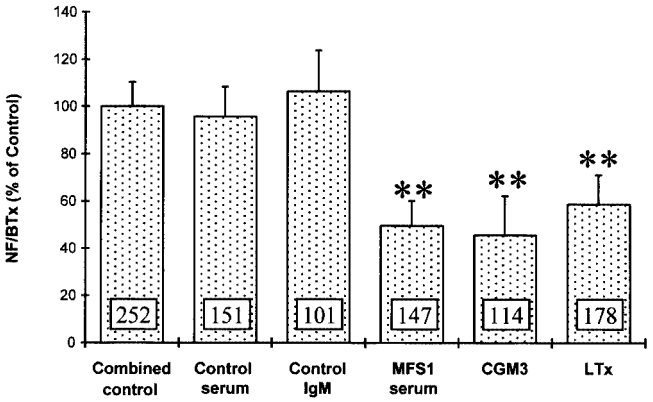

Fig. 4 Image analysis of the NF signal obtained at the mouse NMJ with an anti-phosphorylated NF antibody (1211) on control and anti-GQ1b antibody-treated hemi-diaphragms. The results are the combined data from four separate analyses, and are expressed as a percentage of the NF area/BTx area value obtained for the combined control tissue (mean + standard error of the mean). Compared with the control, the amount of the NMJ covered by NF was significantly reduced (Student's one-tailed *t*-test: $^{**}P < 0.01$) in anti-GQ1b antibody-treated samples. Sample size (n NMJs) is given in boxes.

Alkaline phosphatase treatment

To exclude the possibility that the changes observed in anti-NF antibody binding at NMJs were due to alterations in the phosphorylation state of the filaments, rather than physical degradation of the immunoreactive epitopes, sections of normal tissue were treated overnight with alkaline phosphatase and stained with antibodies to NF. When quantified, the signal from antibody 2F11 (phosphorylated-NF) was significantly reduced compared with untreated NMJs, while that from 1217 (non-phosphorylated-NF) was significantly increased (Fig. 5). However, anti-GQ1b mAb CGM3-treated tissue, having a lower NF signal than control tissue, showed no significant recovery of 1217 staining following alkaline phosphatase treatment (Fig. 5), indicating that changes in phosphorylation status could not account for the loss of NF staining.

β-Tubulin changes at the NMJ

The loss of β-tubulin at the NMJ was investigated in fixed diaphragm tissue from the series of hemi-diaphragm preparations used for the NF staining above. Compared with controls, staining for β-tubulin was significantly reduced ($P < 0.01$) at the NMJ in CGM3- and LTx-treated tissue, but not in MFS1-treated tissue (Fig. 6).

Ultrastructural correlates of gross morphological changes

A total of 110 NMJs were sampled in the EM analysis, consisting of five to 12 NMJs from each hemi-diaphragm. Data for individual NMJs are summarized in Table 1. Data for NMJs from the two control groups (mAb 22/18 and

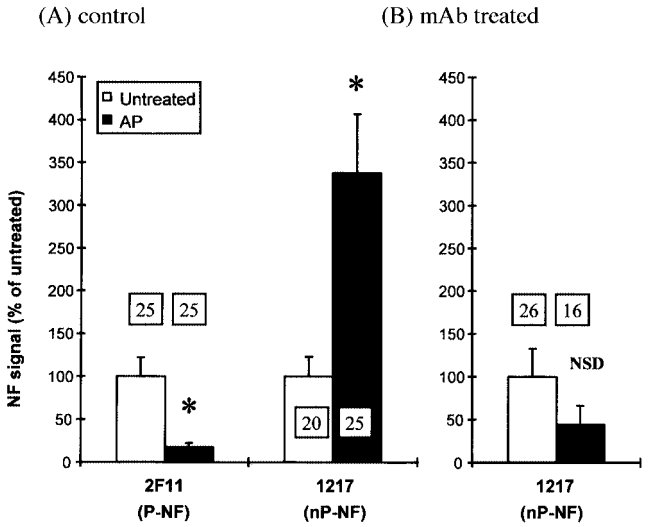

Fig. 5 The effect of alkaline phosphatase (AP) treatment on the immunolabelling signal obtained with antibodies specific for different NF phosphorylation states. (**A**) In control tissue, AP treatment significantly reduces the signal from an anti-phosphorylated NF (P-NF) antibody (2F11), and increases that of an anti-non-phosphorylated NF (nP-NF) antibody (1217). (**B**) In CGM3-treated tissue, the already low NF signal (typically ~40% of controls; hidden by normalization to 100%) seen using 1217 was not significantly increased following treatment, indicating that the loss is not due to changes in phosphorylation state. Values are mean + standard error of the mean. Statistics are based on the Student's one-tailed *t*-test; $*P < 0.05$. NSD = no significant difference. Sample size (*n* NMJs) is given in boxes.

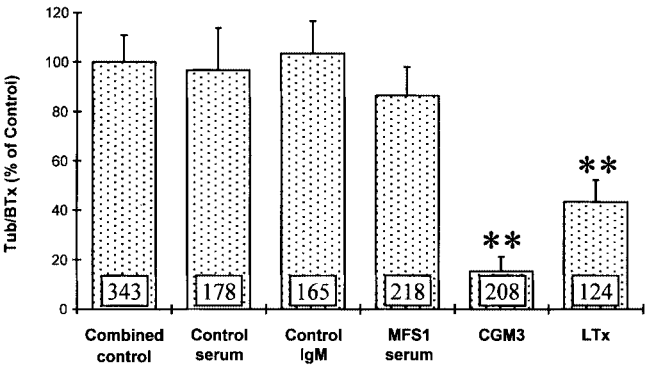

Fig. 6 Analysis of β-tubulin immunostaining at NMJs in hemi-diaphragm preparations. There is a significant loss of β-tubulin staining in CGM3- and LTx-treated tissue, but MFS1-treated tissue did not differ from control levels. Statistics are based on the Student's one-tailed *t*-test; $**P < 0.01$. Sample size (*n* NMJs) is given in boxes.

normal human serum) were not found to be significantly different, and for simplification, statistical tests analysed the pooled data from these two groups. Ninety-two per cent of the NMJs in hemi-diaphragms exposed to control antibody were determined as having an overall normal morphology: all mitochondria were electron dense with well-defined cristae, and nerve terminals were positioned over JF (Fig. 7). Completely denervated NMJs (i.e. with no neuronal structures in close opposition to the post-synaptic apparatus) were not observed in control tissue. The number of NMJs described as normal was significantly lower in MFS1-, CGM3- or LTx-treated tissue compared with controls. In LTx- and CGM3-treated tissue, 0 and 5% (1 NMJ), respectively, were classified as normal, compared with 28% (7/25) of MFS1-treated NMJs. The MFS1-treated NMJs assigned as 'normal' (MFS1normal) were not significantly different from the pooled controls in any of the whole NMJ parameters, whereas the MFS1-treated NMJs assigned as 'abnormal' (MFS1abnormal) did not differ from CGM3-treated NMJs. Thus, rather than exhibiting a gradient of injury, two clear populations of nerve terminals appeared to be present in MFS1-treated tissue. Experimental antibody- or LTx-treated nerve terminals frequently contained mitochondria that appeared swollen, but for the purposes of this study only those mitochondria demonstrating highly abnormal, deteriorating or absent cristae were scored as damaged (Fig. 7). In total, 74% of CGM3-, MFS1- and LTx-treated NMJs had damaged mitochondria. There was no difference between these different experimental subgroups for this parameter. In CGM3- or MFS1-treated NMJs, the incidence of nerve terminal profiles with a full wrap of Schwann cell processes was significantly greater than either LTx- or control antibody-treated tissue. Denervated NMJs, i.e. with no nerve terminal structures in contact with JF, were seen in MFS1- and CGM3-treated tissue, but not in LTx-treated tissue.

The pre-synaptic region of individual NMJs was represented by one or more nerve terminal profiles and a total of 329 nerve profiles was thus analysed from the 110 NMJs. The data for individual profiles are also summarized in Table 1. In normal NMJs, the nerve terminal comprises finger-like processes which, if cut transversely, give a rounded profile, whilst longitudinal sectioning produces a more elongated profile. As such, the profile perimeter is inversely proportional to profile circularity (Spearman's rank correlation coefficient $\rho s = -0.68$; Fig. 8). The proportion of the profile in contact with the muscle (expressed as the muscle contact ratio), 0.43 ± 0.01 (mean ± SEM) was relatively constant, but correlated weakly with perimeter length ($\rho s = 0.32$; data not shown). Schwann cell processes inserting into the synaptic cleft between the terminal and an associated junctional fold, or completely enveloping the terminal were rarely observed in control tissue.

Compared with control antibody-treated tissues, CGM3-treated nerve terminal profiles were significantly more likely to have Schwann cell processes partially or completely separating them from the post-synaptic apparatus. In addition, the mean perimeter length and muscle contact ratio of profiles were both significantly smaller, and circularity significantly greater than control values (Fig. 8). This was due, in part, to the loss or fragmentation of large elongated terminal profiles, and, in part, to an increase in the circularity of smaller ones, since profiles with a perimeter of 1–8 μm had a significantly increased circularity compared with controls (data not shown). Within the terminal itself, damaged mitochondria were frequently observed and, consistent with the exocytic effect

Table 1 *Ultrastructural and morphological data for individual NMJs*

	Pooled controls	MFS1			CGM3	LTx
		Total	Normal	Abnormal		
Whole NMJ						
n	51	25	7	18	22	12
Normal NMJ (%)	92 ± 4*,†	28 ± 9‡	100 ± 0*	0‡	5 ± 5‡	0‡
Damaged mit. (%)	0*,†	68 ± 10‡	0*	94 ± 6‡	73 ± 10‡	92 ± 8‡
Full wrap (%)	8 ± 4†	60 ± 10*,‡	0	83 ± 9*‡	82 ± 8*,‡	17 ± 11†
Denervated (%)	0†	32 ± 10‡	0	44 ± 12*,‡	18 ± 8‡	0
Individual nerve profiles						
n	136	62	16	46	106	25
Perimeter (μm)	8.7 ± 0.4	6.4 ± 0.4*,†,‡	8.4 ± 1.3*,†	5.8 ± 0.3*,‡	4.9 ± 0.2*,‡	20.1 ± 3.3†,‡
MCR	0.43 ± 0.01	0.20 ± 0.03‡	0.43 ± 0.02*,†	0.13 ± 0.03*,‡	0.19 ± 0.02‡	0.29 ± 0.04‡
Circularity	0.38 ± 0.01	0.51 ± 0.02‡	0.39 ± 0.04†	0.55 ± 0.02*,‡	0.54 ± 0.02*,‡	0.42 ± 0.04†
Damaged mit. (% profiles)	0	57 ± 7‡	0	76 ± 7	56 ± 6	81 ± 9
Damaged mit. (% of total)	0	35 ± 5‡	0*†	47 ± 6‡	40 ± 5‡	43 ± 7‡
SC over JF	5 ± 2	39 ± 6‡	0*†	52 ± 7‡	37 ± 5‡	28 ± 9‡
Full wrap (%)	3 ± 1	47 ± 6*,‡	0†	63 ± 7*,‡	45 ± 5*‡	12 ± 7†
Vesicles per 200 ×200 nm box	13.0 ± 0.3	8.2 ± 1.0*‡	12.8 ± 0.8*,†	3.8 ± 0.9‡	6.0 ± 0.5*‡	3.1 ± 0.6†,‡

mit. = mitochondria, MCR = muscle contact ratio, SC = Schwann cell, JF = junctional folds. Statistics: one-tailed *t*-test based on pooled data from each condition. *Significantly different from LTx ($P < 0.01$); †significantly different from CGM3 ($P < 0.01$); ‡significantly different from pooled control ($P < 0.01$).

of the electrophysiological lesion, vesicle counts at the presynaptic membrane were ~50% of control values. Nerve terminal profiles from MFS1 normal NMJs did not differ from those of controls, whilst MFS1 abnormal NMJs were statistically similar to CGM3-treated tissue.

The nerve terminal profiles from LTx-treated NMJs differed from both controls and CGM3-treated tissue. The most striking feature was the massively swollen nerve terminals, with electron-lucent contents (Fig. 7), the mean perimeter being more than twice that of controls. As with CGM3-treated tissue, damaged mitochondria were common. However, in contrast, the incidence of Schwann cell processes forming full wraps around profiles was similar to controls. Vesicle density was significantly lower than control and CGM3-treated tissue.

Discussion

These data show that polyclonal anti-GQ1b antibody containing serum from an MFS patient and a mouse monoclonal anti-GQ1b antibody (CGM3) are able to activate human complement and cause morphological destruction of the motor nerve terminal in the *ex vivo* mouse hemi-diaphragm preparation, in addition to causing the electrophysiological lesions described previously (Goodyear *et al.*, 1999; Plomp *et al.*, 1999; Bullens *et al.*, 2000). As well as being a pathophysiological mechanism that possibly contributes to the paralytic features of MFS, degeneration of the nerve-terminal and distal motor nerve may also, in part, underlie the motor features of other anti-ganglioside antibody-associated neuropathies, as has been suggested previously (Ho *et al.*, 1997).

Anti-NF antibody binding is influenced by the NF phosphorylation state, which is determined by many factors including the intracellular location. In general, non-phosphorylated NF is associated with cell bodies, dendrites and proximal axons, whereas phosphorylated NF is associated with stable, compacted regions of the axon (Sternberger and Sternberger, 1983). Both phosphorylated and non-phosphorylated NF have been demonstrated at the NMJ (Donahue *et al.*, 1988; Greenwood *et al.*, 1993; Plomp *et al.*, 1999). Loss of NF immunostaining arising as a result of changes in the phosphorylation state, particularly increased phosphorylation within the cell body, has been reported as a marker of CNS disease or injury (Bizzi and Gambetti, 1986; Hugon and Vallat, 1990; Nakazato *et al.*, 1990; Giasson and Mushynski, 1996; Laskawi and Wolff, 1996). The loss of both phosphorylated and non-phosphorylated NF in the system described here, in conjunction with the failure of alkaline phosphatase to recover non-phosphorylated NF and the loss of β-tubulin staining, indicates that physical disruption or destruction of elements of the intra-terminal cytoskeleton has occurred.

The ultrastructural analysis of lesions resulting in denervation requires a quantitative approach, as a variety of 'abnormal' morphological states may also be found in normal tissue. These may represent the naturally occurring, low-frequency process of denervation and re-innervation, which becomes more common with increasing age and with changes in muscle usage (Fahim, 1989; Boaro *et al.*, 1998). Also, in this *ex vivo* analysis, transection of the phrenic nerve during tissue dissection may induce downstream changes at the NMJ. Studies in the rat have shown that major morphological changes are evident at some diaphragm NMJs after 6–12 h following phrenic nerve transection *in vivo* (Miledi and Slater, 1970; Manolov, 1973). In our studies, the hemi-diaphragm

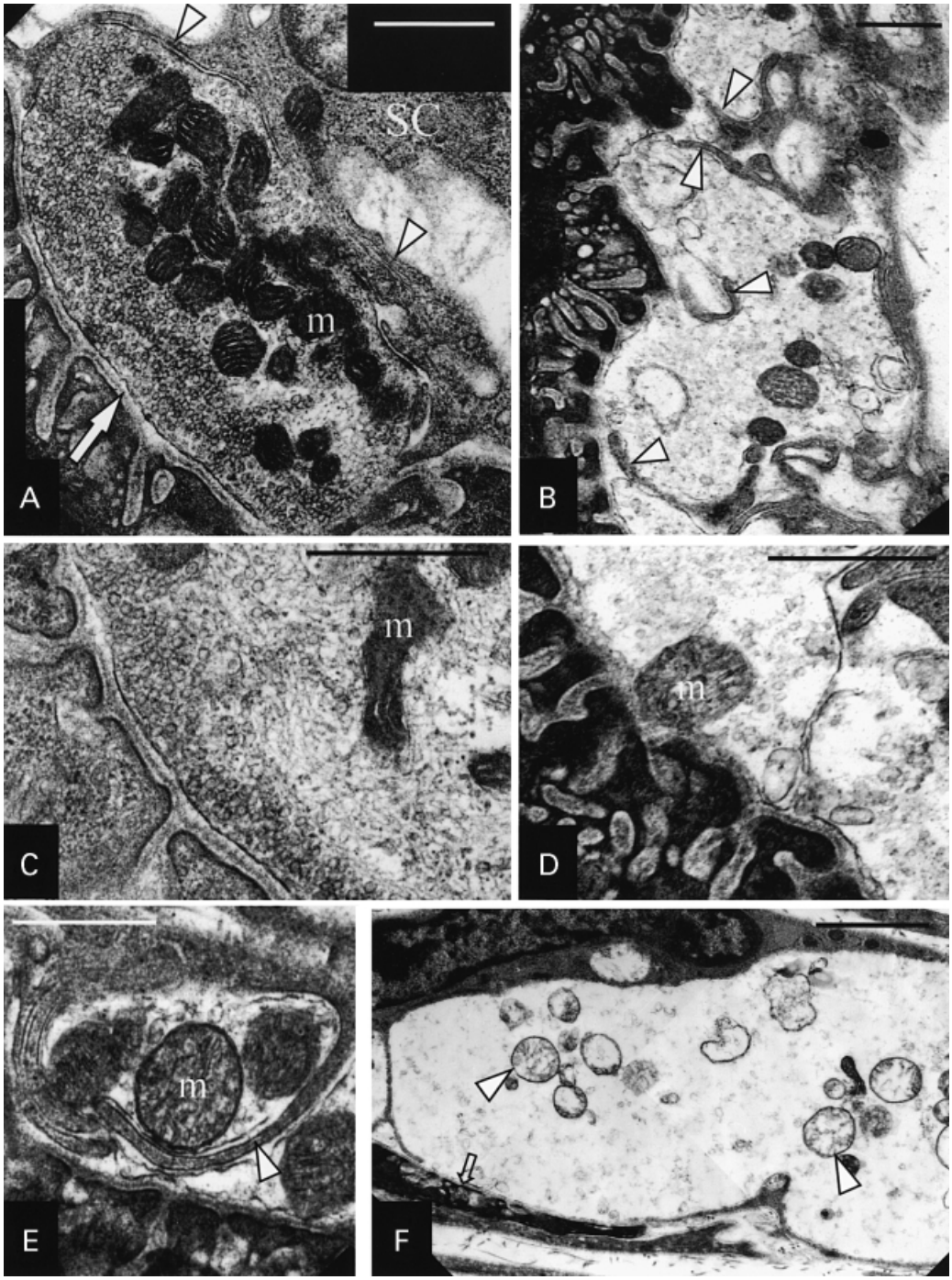

Fig. 7 Ultrastructural features of control and anti-GQ1b mAb-treated tissue. (**A**) Control antibody-treated NMJ. The pre-synaptic region of the terminal is filled with closely packed synaptic vesicles. Mitochondria (m) stain darkly, and have well defined and closely apposed cristae. The basal lamina is visible both within the synaptic cleft (arrow), and extending down between individual junctional folds. A capping Schwann cell (SC) extends processes (arrowheads) over the surface of the terminal, but these do not extend into the synaptic cleft. Scale bar = 600 nm. (**B**) Anti-GQ1b mAb CGM3-treated NMJ. The nerve terminal is more electron-lucent than in controls, due, at least in part, to a reduction in vesicle density. A series of Schwann cell processes (arrowheads) appear to be fragmenting the terminal. Scale bar = 600 nm. (**C** and **D**) Compared with control antibody-treated NMJs (**C**), anti-GQ1b antibody CGM3-treated NMJs (**D**) show a lower density of synaptic vesicles close to the pre-synaptic membrane, and there is little evidence of the cytoskeletal meshwork within the nerve terminal. Scale bars = 600 nm. (**E**) Anti-GQ1b antibody CGM3-treated NMJs in which Schwann cell processes (arrowheads) have formed a full wrap around part of the nerve terminal. Scale bar = 600 nm. (**F**) LTx-treated NMJs appeared extremely swollen and electron-lucent, and the post-synaptic junctional folds (arrow) were flattened. Clusters of mitochondria (arrowheads) in an advanced state of degeneration are evident within the nerve terminal. Scale bar = 1.8 μm.

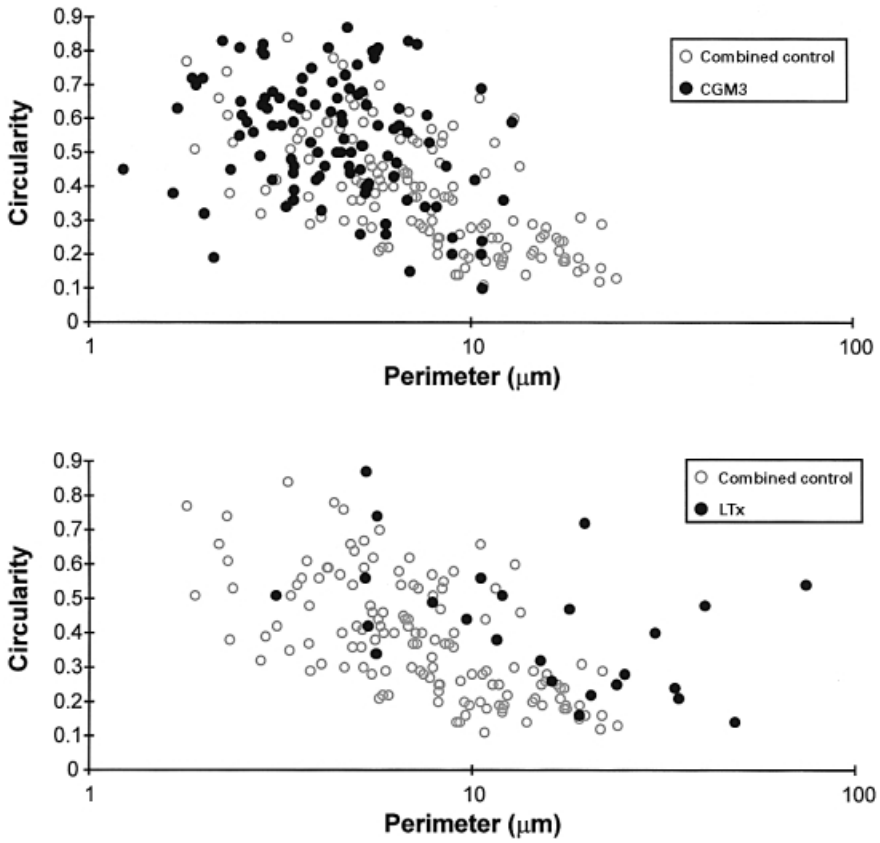

Fig. 8 The relationship between perimeter length and circularity (an image analysis function determining the approximation to a circle) in nerve terminal profiles from CGM3-treated, LTx-treated and combined control tissue. In control tissue there was an inverse relationship between the two parameters. Treatment with CGM3 resulted in the loss of large perimeter profiles, and an increase in the circularity of smaller ones. Conversely, LTx treatment, which caused the terminals to swell, resulted in much higher perimeters. Statistical comparisons based on these data are displayed in Table 1.

was maintained *ex vivo* at room temperature for ~4.5 h in good physiological condition, as judged by the sustained tetanic contraction upon nerve stimulation. It is, however, possible that phrenic nerve transection may to some extent contribute to the evolution of abnormalities observed in these experiments, reinforcing the need for quantitative comparisons between control and experimental antibody-treated tissues. We were able to quantify a range of morphological characteristics that are significantly different between control and anti-ganglioside antibody-treated tissues (Table 1), and which are supported by the immunohistological observation of NMJ cytoskeletal loss. In CGM3-treated tissue, the vast majority of NMJs displayed abnormalities of the nerve terminal, including damaged mitochondria and a reduced contact with the associated muscle. In addition, signs of cell process infiltration into the NMJ were common; these were confirmed as Schwann cells rather than macrophages by the presence of a basal lamina on their outer surface. A significant number of nerve terminal profiles were completely encased by a 'full wrap' of Schwann cell processes, and the nerve terminal appeared to be broken up into smaller units by invading processes, attested to by the reduced perimeter of these profiles. Many more nerve terminals had Schwann cell processes intruding into the synaptic cleft. Thus, it appears that the Schwann cell plays an important role in the breakdown of the nerve terminal in this model. Our work and that of others (Duchen *et al.*, 1981) suggests that at least in the very early stages of evolution of the LTx lesion, Schwann cells are considerably less active than in anti-GQ1b antibody- and complement-treated tissue. Thus, 90 min after application of LTx, at a time when there was very extensive terminal swelling, vesicle depletion and mitochondrial damage, the incidence of Schwann cell processes forming a full wrap around the terminal was not different from controls. Sublytic doses of terminal complement complexes are able to trigger metabolic changes within Schwann cells (Dashiell and Koski, 1999; Dashiell *et al.*, 1999) and it is likely that such cells are recruited into the degenerative process and become phagocytic at a much earlier stage if they are already in close association with a site of complement activation.

In CGM3-treated tissue, the great majority of NMJ showed signs of severe damage, as judged by all measured parameters (i.e. functional scoring, C3c deposition, NF and β-tubulin loss and ultrastructural changes). However, in MFS1-treated

tissue, abnormalities in these parameters were more heterogeneously distributed, indicating either a milder and/or less advanced lesion had evolved at the time of analysis, or that a subgroup of NMJ were selectively vulnerable. Such selectivity could be due to many factors, including differences in ganglioside antigen density or distribution, or differences related to muscle fibre type (Frey *et al.*, 2000). Furthermore, we cannot assume that the abnormalities in all the parameters we measured either evolve contemporaneously or are triggered similarly, which again could be due to diverse factors. In CGM3-treated tissue, NF and β-tubulin loss were both evident at the time of sampling, whereas in MFS1-treated tissue, NF and β-tubulin loss were dissociated, as has been observed previously following head injury (McCracken *et al.*, 1999).

Both the pathological changes we observed in this study and the electrophysiological data from previous work are similar to the changes observed at the NMJ following exposure to either α-latrotoxin or β-bungarotoxin (Dixon and Harris, 1999). Since these toxins are thought to mediate their effects through different mechanisms (Rowan and Harvey, 1988; Ueno and Rosenberg, 1990; Henkel and Sankaranarayanan, 1999), it is clear that destruction of the motor nerve terminal and pre-terminal axon occurs secondarily to a variety of NMJ injuries. The mechanism by which anti-GQ1b antibodies and complement produce a primary lesion at the NMJ may be different from either of these neurotoxins. However, we predict that in all these cases, the loss of nerve terminal integrity leads to the activation of intra-terminal proteases that destroy the cytoskeleton and lead to nerve retraction. The mechanism by which this occurs in this model remains incompletely understood. The destructive process may be secondary to the electrophysiological effect, possibly due to the extremely high rate of exocytosis. In support of this, the exocytic effect starts to occur 1–5 min following the addition of complement to tissues incubated with anti-GQ1b mAbs, whereas NF abnormalities are first apparent by immunostaining after 15–30 min (our unpublished observations).

Complement activation has been shown to alter the permeability of synaptosomal preparations of nerve terminals (Schweitzer and Blaustein, 1980), and this is likely to be due, at least in part, to the formation of the terminal membrane attack complex. This pore-forming structure allows an influx of ions including Ca^{2+}, and thus the upregulation of Ca^{2+}-dependent processes, including activation of the protease calpain. Both NF and tubulin are calpain substrates and therefore the loss of immunostaining is in keeping with this hypothesis. Phosphorylated NF, common in axons, is more resistant to calpain cleavage than non-phosphorylated NF (Pant, 1988). If calpain is a key mediator of cytoskeletal breakdown, this may explain why in this hemi-diaphragm model, large intramuscular nerve bundles retain NF immunostaining while the nerve terminals are destroyed. However, axonal NF staining was not quantified in this study, and therefore the degree to which such complement-mediated nerve-terminal damage may spread proximally into the pre-terminal axon and beyond remains unknown. There are degenerative changes in the pre-terminal axon of the NMJ shown in Fig. 1B, and it is possible that this initially focal lesion could lead to more extensive proximal spreading of the pathological process into the distal motor nerve, given sufficient time. Supporting this idea is the observation that in muscles envenomed with β-bungarotoxin, NF immunostaining was lost in intramuscular nerve bundles as well as at the NMJ (Dixon and Harris, 1999).

From our previous studies using complement-deficient sera, it appears that the electrophysiological effects produced by anti-GQ1b mAbs and complement continued in the absence of membrane attack complex formation (Plomp *et al.*, 1999), but we do not know whether cytoskeletal damage was evident in these studies. Using complement factor deficient sera we determined previously that the electrophysiological blocking effects could not occur in the absence of C5, but could occur in the absence of C6, indicating a possible role for the anaphylotoxin C5a (Plomp *et al.*, 1999). Interestingly, C5-deficient mice also display delayed Wallerian degeneration (Liu *et al.*, 1999), which may point to a role for the activation products of this factor in normal neuronal restructuring and repair. Receptors to the C5-derived anaphylatoxin, C5a, are present on neurones (Stahel *et al.*, 1997), and this ligand induces apoptosis in neuroblastoma cells (Farkas *et al.*, 1998). As such, a C5a receptor-transduced pathway may underlie the morphological and/or electrophysiological effects caused by anti-GQ1b antibodies and complement. Equally, this does not exclude a role for membrane attack complex in mediating advanced pathophysiological stages of this injury.

Irrespective of the mechanism triggering the initial lesion, it appears that phagocytic cells are recruited that contribute to the retraction of nerve terminals away from the NMJ. Whereas in our study the presence of a basal lamina indicated that these were Schwann cells, we cannot preclude and indeed expect, a role for macrophages at later time-points in this process, if it were to occur *in vivo*.

Since the paralytic features of MFS involve only a small subset of muscles, further complexity may be generated at other levels. This hemi-diaphragm model has been optimized by the use of heterologous complement, which may circumvent some of the host complement regulatory mechanisms involved in clearance or inactivation of complement products. We know that mouse serum, when used as a source of complement, is unable to mediate these effects under equivalent incubation conditions (J. J. Plomp and R. W. M. Bullens, unpublished observations). With a homologous complement source, as occurs in human with MFS, only NMJs or other neural structures with a particularly high GQ1b antigen density may succumb to neural injury. The human extraocular nerves, which are enriched in GQ1b (Chiba *et al.*, 1997), may therefore be particularly vulnerable to this antibody-mediated effect.

Our study provides clear evidence of morphological

destruction of motor nerve terminals resulting from the complement activation produced by anti-GQ1b antibody binding. Whilst recognizing that it remains unproven whether this faithfully represents any elements of the immunopathology of MFS, these data nevertheless provide further evidence to support the notion that anti-ganglioside antibodies, present in the serum of patients with autoimmune neuropathy, have important pathophysiological potential.

Acknowledgements

The authors wish to thank Mrs S. Kerr and Mr W. Smith for their highly proficient technical assistance. We also wish to thank the Trustees of the William Ramsay Henderson Trust for the award of a travelling scholarship to G.M.O'H., which made the collaborative study at the Cleveland Clinic possible. This work was supported by grants from the Wellcome Trust and the GBS Support Group (UK). M.C. received a vacation scholarship from the Wellcome Trust and H.J.W. is a Wellcome Trust Research Leave Fellow.

References

Billger M, Wallin M, Karlsson J-O. Proteolysis of tubulin and microtubule-associated proteins 1 and 2 by calpain I and II. Difference in sensitivity of assembled and disassembled microtubules. Cell Calcium 1988; 9: 33–44.

Bizzi A, Gambetti P. Phosphorylation of neurofilaments is altered in aluminium intoxication. Acta Neuropathol (Berl) 1986; 71: 154–8.

Boaro SN, Soares JC, Konig B Jr. Comparative structural analysis of neuromuscular junctions in mice at different ages. Anat Anz 1998; 180: 173–9.

Buchwald B, Weishaupt A, Toyka KV, Dudel J. Immunoglobulin G from a patient with Miller-Fisher syndrome rapidly and reversibly depresses evoked quantal release at the neuromuscular junction of mice. Neurosci Lett 1995; 201: 163–6.

Buchwald B, Weishaupt A, Toyka KV, Dudel J. Pre- and postsynaptic blockade of neuromuscular transmission by Miller-Fisher syndrome IgG at mouse motor nerve terminals. Eur J Neurosci 1998; 10: 281–90.

Bullens RWM, O'Hanlon GM, Goodyear CS, Molenaar PC, Conner J, Willison HJ, et al. Anti-GQ1b antibodies and evoked acetylcholine release at mouse motor endplates. Muscle Nerve 2000; 23: 1035–43.

Chiba A, Kusunoki S, Shimizu T, Kanazawa I. Serum IgG antibody to ganglioside GQ1b is a possible marker of Miller Fisher syndrome. Ann Neurol 1992; 31: 677–9.

Chiba A, Kusunoki S, Obata H, Machinami R, Kanazawa I. Serum anti-GQ1b IgG antibody is associated with ophthalmoplegia in Miller Fisher syndrome and Guillain-Barre syndrome: clinical and immunohistochemical studies. Neurology 1993; 43: 1911–7.

Chiba A, Kusunoki S, Obata H, Machinami R, Kanazawa I. Ganglioside composition of the human cranial nerves, with special reference to pathophysiology of Miller Fisher syndrome. Brain Res 1997; 745: 32–6.

Dashiell SM, Koski CL. Sublytic terminal complement complexes decrease PO gene expression in Schwann cells. J Neurochem 1999; 73: 2321–30.

Dashiell SM, Rus H, Koski CL. Membrane attack complex of complement (C5b9) induces proliferation and rescue from apoptosis of Schwann cells (SchC). J Periph Nerv Sys 1999; 4: 174.

de Freitas MS, de Mattos-Dutra A, Wannmacher CM, Pessoa-Pureur R. Ca2+-mediated phosphorylation and proteolysis activity associated with the cytoskeletal fraction from cerebral cortex of rats. Neurochem Res 1996; 21: 1489–95.

Dixon RW, Harris JB. Nerve terminal damage by beta-bungarotoxin: its clinical significance. Am J Pathol 1999; 154: 447–55.

Donahue SP, Wood JG, English AW. On the role of the 200-kDa neurofilament protein at the developing neuromuscular junction. Dev Biol 1988; 130: 154–66.

Duchen LW, Gomez S, Queiroz LS. The neuromuscular junction of the mouse after black widow spider venom. J Physiol (Lond) 1981; 316: 279–91.

Fahim MA. Rapid neuromuscular remodeling following limb immobilization. Anat Rec 1989; 224: 102–9.

Farkas I, Baranyi L, Liposits ZS, Yamamoto T, Okada H. Complement C5a anaphylatoxin fragment causes apoptosis in TGW neuroblastoma cells. Neuroscience 1998; 86: 903–11.

Fishman PH, Pacuszka T, Orlandi PA. Gangliosides as receptors for bacterial enterotoxins. [Review]. Adv Lipid Res 1993; 25: 165–87.

Frey D, Schneider C, Xu L, Borg J, Spooren W, Caroni P. Early and selective loss of neuromuscular synapse subtypes with low sprouting competence in motoneuron diseases. J Neurosci 2000; 20: 2534–42.

Giasson BI, Mushynski WE. Aberrant stress-induced phosphorylation of perikaryal neurofilaments. J Biol Chem 1996; 271: 30404–9.

Goodyear CS, O'Hanlon GM, Plomp JJ, Wagner ER, Morrison I, Veitch J, et al. Monoclonal antibodies raised against Guillain Barré syndrome-associated Campylobacter jejuni lipopolysaccharides react with neuronal gangliosides and paralyze muscle-nerve preparations. J Clin Invest 1999; 104: 697–708.

Greenwood JA, Troncoso JC, Costello AC, Johnson GV. Phosphorylation modulates calpain-mediated proteolysis and calmodulin binding of the 200-kDa and 160-kDa neurofilament proteins. J Neurochem 1993; 61: 191–9.

Henkel AW, Sankaranarayanan S. Mechanisms of alpha-latrotoxin action. [Review]. Cell Tissue Res 1999; 296: 229–33.

Ho TW, Hsieh S-T, Nachamkin I, Willison HJ, Sheikh K, Kiehlbauch J, et al. Motor nerve terminal degeneration provides a potential mechanism for rapid recovery in acute motor axonal neuropathy after Campylobacter infection. Neurology 1997; 48: 717–24.

Hugon J, Vallat JM. Abnormal distribution of phosphorylated neurofilaments in neuronal degeneration induced by kainic acid. Neurosci Lett 1990; 119: 45–8.

Jacobs BC, Endtz HP, van der Meché FG, Hazenberg MP, Achtereekte HAM, van Doorn PA. Serum anti-GQ1b IgG antibodies

recognize surface epitopes on Campylobacter jejuni from patients with Miller-Fisher-syndrome. Ann Neurol 1995; 37: 260–4.

Jacobs BC, Hazenberg MP, van Doorn PA, Endtz HP, van der Meché FG. Cross-reactive antibodies against gangliosides and Campylobacter jejuni lipopolysaccharides in patients with Guillain-Barre or Miller Fisher syndrome. J Infect Dis 1997; 175: 729–33.

Kintner CR, Brockes JP. Monoclonal antibodies to the cells of a regenerating limb. J Embryol Exp Morphol 1985; 89: 37–55.

Laskawi R, Wolff JR. Changes in the phosphorylation of neurofilament proteins in facial motoneurons following various types of nerve lesion. ORL J Otorhinolaryngol Relat Spec 1996; 58: 13–22.

Liu L, Lioudyno M, Tao R, Eriksson P, Svensson M, Aldskogius H. Hereditary absence of complement C5 in adult mice influences Wallerian degeneration, but not retrograde responses, following injury to peripheral nerve. J Peripher Nerv Syst 1999; 4: 123–33.

Manolov S. Initial changes in the neuromuscular synapses of denervated rat diaphragm. Brain Res 1974; 65: 303–16.

Masukawa LM, Livengood DR. Alterations in spontaneous transmitter release by divalent cations after treatment of the neuromuscular junction with beta-bungarotoxin. Cell Mol Neurobiol 1982; 2: 277–90.

McCracken E, Hunter AJ, Patel S, Graham DI, Dewar D. Calpain activation and cytoskeletal protein breakdown in the corpus callosum of head-injured patients. J Neurotrauma 1999; 16: 749–61.

Miledi R, Slater CR. On the degeneration of rat neuromuscular junctions after nerve section. J Physiol (Lond) 1970; 207: 507–28.

Nakazato Y, Hirato J, Ishida Y, Hoshi S, Hasegawa M, Fukuda T. Swollen cortical neurons in Creutzfeldt-Jakob disease contain a phosphorylated neurofilament epitope. J Neuropathol Exp Neurol 1990; 49: 197–205.

Pant HC. Dephosphorylation of neurofilament proteins enhances their susceptibility to degradation by calpain. Biochem J 1988; 256: 665–8.

Pashkov V, Grico V, Tsurupa G, Storchak L, Shatursky O, Himmerlreich N, et al. Monoclonal antibodies can uncouple the main alpha-latrotoxin effects: toxin-induced Ca2+ influx and stimulated neurotransmitter release. Neuroscience 1993; 56: 695–701.

Penner JL, Aspinall GO. Diversity of lipopolysaccharide structures in Campylobacter jejuni. [Review]. J Infect Dis 1997; 176 Suppl 2: S135–8.

Plomp JJ, Molenaar PC, O'Hanlon GM, Jacobs BC, Veitch J, Daha MR, et al. Miller Fisher anti-GQ1b antibodies: α-latrotoxin-like effects on motor end plates. Ann Neurol 1999; 45: 189–99.

Prakash YS, Miller SM, Huang M, Sieck GC. Morphology of diaphragm neuromuscular junctions on different fibre types. J Neurocytol 1996; 25: 88–100.

Roberts-Lewis JM, Siman R. Spectrin proteolysis in the hippocampus: a biochemical marker for neuronal injury and neuroprotection. Ann N Y Acad Sci 1993; 679: 78–86.

Rowan EG, Harvey AL. Potassium channel blocking actions of beta-bungarotoxin and related toxins on mouse and frog motor nerve terminals. Br J Pharmacol 1988; 94: 839–47.

Salloway S, Mermel LA, Seamans M, Aspinall GO, Nam Shin JE, Kurjanczyk LA, et al. Miller-Fisher syndrome associated with Campylobacter jejuni bearing lipopolysaccharide molecules that mimic human ganglioside GD3. Infect Immun 1996; 64: 2945–9.

Schweitzer ES, Blaustein MP. The use of antibody and complement to gain access to the interior of presynaptic nerve terminals. Exp Brain Res 1980; 38: 443–53.

Seubert P, Ivy G, Larson J, Lee J, Shahi K, Baudry M, et al. Lesions of entorhinal cortex produce a calpain-mediated degradation of brain spectrin in dentate gyrus. I. Biochemical studies. Brain Res 1988; 459: 226–32.

Siman R, Baudry M, Lynch G. Brain fodrin: substrate for calpain I, an endogenous calcium-activated protease. Proc Natl Acad Sci USA 1984; 81: 3572–6.

Stahel PF, Kossmann T, Morganti-Kossmann MC, Hans VH, Barnum SR. Experimental diffuse axonal injury induces enhanced neuronal C5a receptor mRNA expression in rats. Brain Res Mol Brain Res 1997; 50: 205–12.

Sternberger LA, Sternberger NH. Monoclonal antibodies distinguish phosphorylated and nonphosphorylated forms of neurofilaments in situ. Proc Natl Acad Sci USA 1983; 80: 6126–30.

Suzuki T, Chiba A, Kusunoki S, Chikuda M, Fujita T, Misu K. Anti-GQ1b ganglioside antibody and ophthalmoplegia of undetermined cause. Br J Opthalmol 1998; 82: 916–8.

Ueno E, Rosenberg P. Inhibition of phosphorylation of rat synaptosomal proteins by snake venom phospholipase A2 neurotoxins (beta-bungarotoxin, notexin) and enzymes (Naja naja atra, Naja nigricollis). Toxicon 1990; 28: 1423–37.

Uncini A, Lugaresi A. Fisher syndrome with tetraparesis and antibody to GQ1b: evidence for motor nerve terminal block. Muscle Nerve 1999; 22: 640–4.

Willison HJ, Veitch J, Paterson G, Kennedy PG. Miller Fisher syndrome is associated with serum antibodies to GQ1b ganglioside. J Neurol Neurosurg Psychiatry 1993; 56: 204–6.

Willison HJ, Almemar A, Veitch J, Thrush D. Acute ataxic neuropathy with cross-reactive antibodies to GD1b and GD3 gangliosides. Neurology 1994; 44: 2395–7.

Willison HJ, O'Hanlon GM, Paterson G, Veitch J, Wilson G, Roberts M, et al. A somatically mutated human antiganglioside IgM antibody that induces experimental neuropathy in mice is encoded by the variable region heavy chain gene, V1–18. J Clin Invest 1996; 97: 1155–64.

Yee WC, Pestronk A, Alderson K, Yuan CM. Regional heterogeneity in the distal motor axon: three zones with distinctive intrinsic components. J Neurocytol 1988; 17: 649–56.

Yuki N. Anti-ganglioside antibody and neuropathy: review of our research. J Periph Nerv Sys 1998; 3: 3–18.

Yuki N, Taki T, Takahashi M, Saito K, Yoshino H, Tai T, et al. Molecular mimicry between GQ1b ganglioside and lipopolysaccharides of Campylobacter jejuni isolated from patients with Fisher's syndrome. Ann Neurol 1994; 36: 791–3.

Zalman LS, Muller-Eberhard HJ. Comparison of channels formed by poly C9, C5b-8 and the membrane attack complex of complement. Mol Immunol 1990; 27: 533–7.

Received March 31, 2000. Revised November 11, 2000.
Second revision January 2, 2001. Accepted January 5, 2001